2011

Enhanced Interlayer Exchange Coupling in Co/Fe/MgO/Fe(001)

Andrew Hoff
Andrews University, hoff@andrews.edu

John Nevins Andrews Scholars
Andrews University Honors Program
Honors Thesis

Enhanced Interlayer Exchange Coupling in Co/Fe/MgO/Fe(001)

Andrew Hoff
April 1, 2011

Primary Advisor: Clark Rowland
Secondary Advisor: Roland Kawakami

Primary Advisor Signature:_____

Department: Physics

Enhanced Interlayer Exchange Coupling in Co/Fe/Mgo/Fe(001)

Andrew Hoff
Andrews University
hoff@andrews.edu

Jared Wong
University of California, Riverside
jwong022@student.ucr.edu

Clark Rowland
Andrews University
rowland@andrews.edu

Roland Kawakami
University of California, Riverside
roland.kawakami@ucr.edu

Abstract

We investigate the bilinear and biquadratic interlayer exchange coupling in Co/Fe/MgO/Fe(001). Samples are grown through molecular beam epitaxy and the interlayer exchange coupling is measured through magneto-optic Kerr effect along wedge samples. By varying the location of Fe impurities between the interface and middle of the MgO spacer, we find that the couplings are enhanced and are dependent on the location of the impurities. We found that the interfacial impurities created a larger impact across all thickness on the bilinear coupling than no impurities or impurities in the middle of the MgO. The biquadratic coupling didn't have a clear trend.

1. Introduction

Magnetic thin films have been a very active area of research since the discovery of giant magnetoresistance (GMR) in 1988. In GMR, two ferromagnetic thin films are separated by a very thin (approx. 1nm) non-ferromagnetic spacing layer. As the magnetic coupling between the two layers changes from parallel to anti-parallel, the resistance of the device changes on the order of 1-10%. This breakthrough led to the development of better hard drive technology, as hard disk drive makers were able to create smaller magnetic sensor heads, which meant that data could be stored more densely on the devices. A related development later was of tunnel magnetoresistance (TMR). This principle is very similar, except that in addition to a non-ferromagnetic spacing layer, it must also be an electrically insulating spacer. The magneto-resistance in TMR can be around an order of magnitude greater than what is attainable with GMR. Since the development of TMR, hard disk drives have been advancing quite markedly, with 3 terabyte hard drives now available.

GMR, and later TMR, were some of the first examples of the new field of spintronics. In spintronics, the quantum mechanical property of spin is utilized. This is either in replacement of, or in addition to, normal electronics which use charge as the fundamental operator. Since spin is integrally tied to the magnetic moment of a particle, many spintronic applications utilize the magnetic properties of materials. One technology that is still in its nascent phases is magnetoresistive random access memory (MRAM). MRAM is based on these magnetic thin film systems. MRAM is a type of computer memory that is non-volatile, meaning it doesn't need power to maintain the memory, it has essentially unlimited read/write cycles, it is expected that it will be more power efficient than other types of memory (particularly compared with flash memory). Currently, it serves a niche market as it can't be shrunk as easily as other types of memory. Current applications are using the memory in some industrial control systems and spacecraft.

One of the main principles involved in these magnetic thin film systems is interlayer exchange coupling[1]. This effect measures the strength of the interaction between the two ferromagnetic layers with the spacer in between. This interaction determines the necessary magnetic field required to change the magnetization of the ferromagnetic layers in the material. A key question concerning this effect is how do impurities in the spacing layer affect the coupling? Since the spacing layer is only a few atoms thick, impurity atoms should have a large impact in the coupling[2345]. Furthermore, does the magnetization of the impurities make any difference to the effect observed?

This research looked at the effects of ferromagnetic impurities in the spacing layer, in particular using Fe as the impurity. We were able to look at samples where there were no impurities added, impurities added at the interface of the spacer, and impurities added in the middle of the spacer. A wedge geometry for the spacer was used so that we could measure across a wide range of thicknesses. While looking at the coupling, we paid attention to the effect of the biquadratic coupling, which had only previously been done with oxygen vacancies[6].

The research was done at University of California Riverside with a graduate student, Jared Wong, and under the supervision of Professor Roland Kawakami.

We grew the samples using molecular beam epitaxy (MBE), characterized the growths using reflection of high energy electron diffraction (RHEED), and measured the samples with a magneto-optic Kerr effect (MOKE) setup. Using a homemade LabVIEW program to analyze the data, we found the strength of the bilinear and biquadratic coupling of the samples.

2. Experimental Procedures

2.1 Molecular Beam Epitaxy

We used MBE for the growth process. We first cleaned and prepared an MgO(001) substrate to grow on. To do this the MgO was first rinsed with de-ionized water and then annealed in ultra-high vacuum at 600 degrees C until the RHEED pattern was good. In RHEED, electrons are reflected off of the material at low angle. The diffraction pattern that forms indicates whether the material grew into a good crystal or whether there were growth defects. The sharper the lines, the better the growth is of the sample. (see Fig. 1). It is important to ensure the good growth of the lattice to avoid much lattice mismatch when subsequent layers are deposited.

We put the substrate in the loading chamber and pumped that down to ultra-high vacuum before moving the sample into the growing chamber. The base pressure for the system was around $1x10^{-10}$ torr. Once the sample is in place, the deposition can occur. Deposition rates were monitored by a quartz sensor residing next to the sample. MBE works in one of two ways. For the MgO, the material was subjected to electron beam evaporation, which causes ejection of the material by bombarding it with electrons. For the remaining materials, a very pure sample of material in a cell undergoes thermal effusion, where it becomes heated and the material sublimates. As the material is ejected from the cell, it disperses in the chamber, with a portion of the materials landing on the growth sample. After the desired amount has been deposited, as determined by the deposition sensor, a screen is placed in front of the sample so that no more material gets deposited on the sample. It is then pumped down once again to ultra-high vacuum and the process is repeated for the remaining materials that need to be deposited. After each layer is deposited, the quality of the growth is checked using RHEED.

To grow the wedges, we covered the cell with the shield, and began evaporating the material in the cell. As the evaporation is occurring, the shield is slowly withdrawn, slowly exposing more of the sample until eventually the entire sample is exposed. The portion of the sample that was exposed the longest is the thickest portion of the wedge, with the part that was uncovered last being the thinnest portion of the wedge.

We were able to grow and measure three samples. The samples generally were grown with a 15 nanometer Fe layer, followed by an MgO wedge, then a 5nm Fe layer, a 50 nm Co layer, and then finally a 10 nm Ag cap to prevent oxidation of the sample as in Fig. 5. For the sample with an interfacial layer of MgO, a small growth of MgO would be deposited before the Fe impurities would be added. For the sample with the impurities in the middle of the MgO layer, the wedge would be grown to be half height of the final structure. The Fe impurities would then be added, and then the final half of the wedge would be grown. In the case of the wedge with the impurities in the middle, this sample was also created as a half/half wedge. Half of the wedge had the impurities in the center, and the other

half had no impurities in the wedge as illustrated in Fig. 6. In both cases with impurities, the Fe layer consists of a ¼ monolayer of Fe. Since this isn't enough to create a one atom thick layer, the material grows in clusters[7]. The no impurity sample grown had significantly different growth characteristics than the other samples, and so the no impurity sample henceforth will refer to the no impurity portion of the half/half wedge.

2.2 Magneto-Optic Kerr Effect

Once the sample is grown, it is measured using a MOKE setup. The setup consisted of a laser beam that was linearly polarized. It was sent through an optical chopper, and then reflected off of the sample. MgO is optically transparent, and so the laser enters through the substrate and is reflected off of the 15 nm Fe layer. Due to the magneto-optic Kerr effect, a linearly polarized beam that gets reflected off of a magnetic material will have its angle of polarization changed depending on the strength of the magnetic field. Once it is reflected, it is broken into vertical and horizontal components and then each beam is turned into an electrical signal by a photodiode bridge.

The sample resides on a holder, and is under the influence of a magnetic field generated by an electromagnet. The sample is put on the holder, with the substrate exposed, and this system is put back into vacuum. The laser is reflected off of the sample. The MgO substrate is optically transparent, so that the reflection is being done by the iron in the sample. After the data is sent to the computer, it is analyzed by a previously made LabVIEW program to analyze the magnetization.

Our measurement procedure was to initially find the thick edge of the sample with the laser. Once the edge had been found, measurements would be taken starting from that edge. A measurement would consist of gradually increasing the current sent to the electromagnet, which in turn increased the magnetic field generated. This magnetic field would rise in steps up to a preset magnetic field, at which point it would reverse and return similarly to the initial conditions. At some applied magnetic field, the "free layer" of Fe, the layer that resides between the substrate and the wedge, will switch its magnetization (if it was initially ferromagnetically coupled with the other iron layer, it will switch to antiferromagnetic coupling and vice versa). The alignment stays constant until the magnetic field eventually reaches a point that the "hard layer" of Fe switches alignment as well. After this happens, the magnetic field will decrease in steps back to the initial conditions. While decreasing the magnetic field, the reverse process will occur as happened when scaling up. However, since the magnetization of the material is path dependent, the switching occurs at different magnetic fields on the way down as on the way up. Because of this path dependence it creates a hysteresis loop, which contains the data necessary to determine the coupling. This process would be done ~5 times and averaged so that the noise would be lessened and features would be clearly visible. Once the data had been taken for the major loop (both the free layer and the hard layer switching), the top magnetic field preset would be changed so that a subsequent set of 10 data runs would be taken and averaged for the minor loop. The minor loop only has the free layer switch before returning back to the initial conditions. It is the minor loop that is

analyzed and from which the information about the coupling is derived. The major loop is useful to see the overall features, as well as to determine what level to set the upper magnetic field limit so that only the free layer is switched. Once the minor loop is determined, the location of the sample is moved so that the laser is reflecting off of a different part of the sample (which would correspond to a different wedge thickness). The process is repeated across the entire length of the sample until the MgO becomes so thin as to make the data unusable. The distance between each measurement depends on the resolution you wish to have, with our measurements occurring every ~.05 nm.

2.3 Data Analysis

Once a minor loop is measured it can be analyzed. A graph of the hysteresis loop for the minor loop is analyzed for every location that was measured. The analysis is done by looking at the shifting and splitting of the rotation vs. the applied magnetic field graphs, which is how the data is presented in the hysteresis loops (Fig. 1). The shifting and splitting of the graph correspond to bilinear and biquadratic coupling, respectively. A shifting of the graph denotes whether the coupling is ferro- or antiferromagnetic. If the center of the loop has moved left of zero, it is antiferromagnetically coupled, while loops centered to the right of zero are ferromagnetically coupled. The splitting of the minor loop shows biquadratic coupling. By measuring the magnitude of the splitting and shifting, one can determine the magnitude of the coupling. The coupling is measured in units of ergs/cm^2, the cgs unit for energy, and is given by

$$J=HM_st \quad (1)$$

where J is the energy of the coupling, H is the experimentally determined distance, M_s is the magnetic moment, and t is the thickness of the material.

3. Results

The data collected is in Figs. 3 and 4. The first and second contain the measurements of the bilinear and biquadratic coupling, respectively. It is clear that impurities can change the coupling strength dramatically.

The bilinear coupling demonstrates that at larger thicknesses, the coupling is ferromagnetic, but at less than ~.8nm MgO thickness it shifts to strongly antiferromagnetic coupling regardless of whether there were impurities. The impurities changed the strength of the antiferromagnetic coupling, and in the case of interfacial impurities doubling the strength of the coupling for a given thickness. Impurities didn't affect the ferromagnetic coupling strength, but it did cause an earlier onset of antiferromagnetic coupling. Above .9nm, there was no, or an imperceptibly small, difference seen in the coupling due to the impurities, with the large differences occurring below .8nm. The interfacial impurity caused the larger change compared with the impurities in the middle of the spacer.

The biquadratic coupling shows an even greater effect due to the impurities. Similarly to bilinear coupling, the large effects occur below .8nm. In contrast, there was a difference above .9nm, with the interfacial impurities actually decreasing the biquadratic coupling at thicknesses above .9nm compared to no impurities and middle of the barrier impurities. Below .8nm, the

presence of impurities greatly increased the biquadratic coupling. The increase seems to get larger with decreasing thickness, with a change of 2-3 times the effect near .6nm. At the very thinnest regions (~.6nm) the middle impurities seem to cause the biggest effect, but between .65 and .8nm interfacial impurities are a bigger contributor to the coupling.

4. Discussion

The data shows that impurities increase the coupling below .8nm. Above that point, it remains unclear whether the differences in the biquadratic coupling were due to actual differences in coupling or variations in the growth process. The fact that it was the no impurity and the middle of the barrier measurements that had very similar changes in the biquadratic coupling suggests that the variation in the coupling above .9nm may be due to an artifact of the growth process (since they were grown on the same sample).

One of the surprising results of this experiment is that the interfacial impurities had the biggest effect on the coupling. Impurities in the middle of the barrier would have been expected to cause stronger coupling, as the barrier is a classically forbidden zone that requires quantum tunneling to cross. Since the probability of tunneling falls off exponentially with increasing distance, it would have the greatest probability of tunneling if there had been an impurity halfway across. Having the impurity at the interface means that nearly the entire distance would need to be crossed in the tunneling.

This result could be due to several possible sources. Since Fe is more electronegative than Mg, at the interfacial impurity the Fe would have most likely completely oxidized the very thin layer of MgO that was put between the free layer and the impurities. It is possible that the FeO/Mg/Fe/MgO/Fe system was more magnetic or susceptible to coupling. Another possibility is that the growth rates were sufficiently different as to cause the two to be incomparable to each other.

One of the difficulties in this experiment is trying to keep the growth process as similar as possible between samples. The electron beam evaporation of the MgO has a potential drawback of breaking the Mg-O bond if the supplied power is too high. As the growth cell gets older and smaller, a higher power is required to get comparable growth rates (which is also important to the structure and characteristics of the sample). We were able to maintain a similar power supplied, but at the expense of having a slower growth rate for the MgO, going from .74 Å to .6 Å on the next growth. This would change the properties of the material, which is why emphasis was placed on the half/half wedge which had the same growing conditions for both the no impurity and the middle of barrier impurities.

5. Subsequent Work

Subsequent work was performed primarily by Jared Wong as he further refined the techniques developed that summer. The wedge geometry was expanded into a double wedge geometry. In this system, the first wedge would be deposited, followed by the impurities, and followed by another wedge rotated 90 degrees from the original wedge. This allowed for a much better resolution of the effects of the thickness of the sample. There was also work in changing the ferromagnetic materials at the interfaces. A

Co/Fe interface was used for the free layer, which markedly improved the coupling. There was a paper published building on the work from that summer as well as subsequent work in Physical Review B in 2010[8].

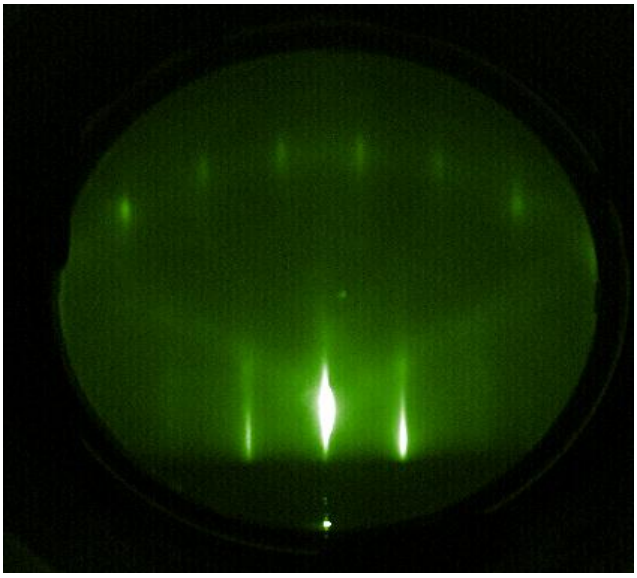

Figure 1- A RHEED image of MgO(100). The sharper the lines are, the better of a crystal structure it has.

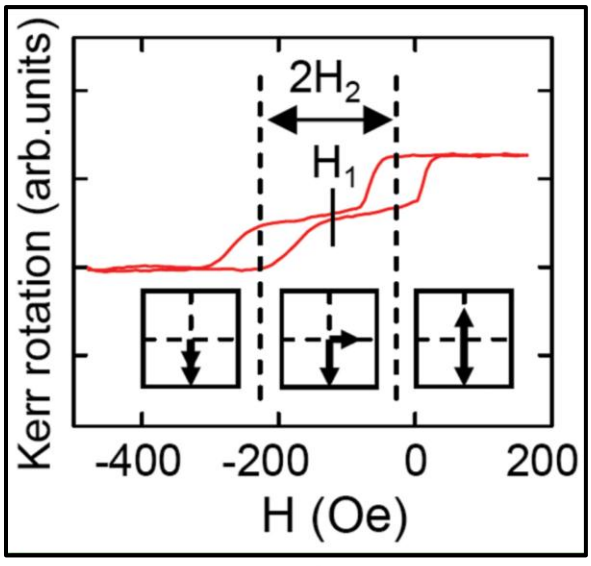

Figure 2- In the loops, the right-hand side of the shape is the path of increasing magnetic field, and the left-hand side is the path of decreasing magnetic field. This example of a minor loop illustrates the two types of coupling. H_1 is the measure of how far the middle of loop has deviated from normal. In this picture, H_1 is around -100 Oe. H_2 is the measure of how much the minor loop has split. The measurement is from the center to either of the endpoints, so by looking at the entirety of the split of the loop from the right- to left-hand side and dividing by two, we would get H_2, which would be around 100 Oe for this loop.

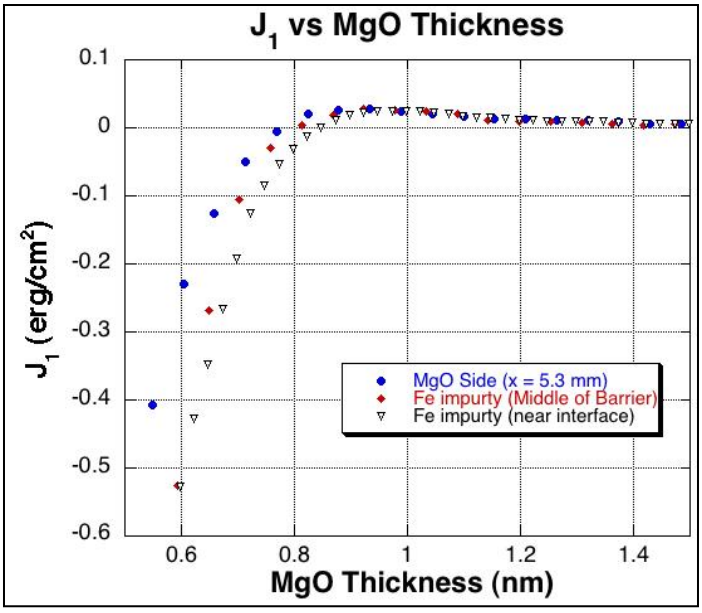

Figure 3- This is a graph of bilinear coupling strength, J_1, versus the thickness of the MgO wedge. Note in particular the change from positive (ferromagnetic coupling) to negative (antiferromagnetic coupling) around .8nm thickness.

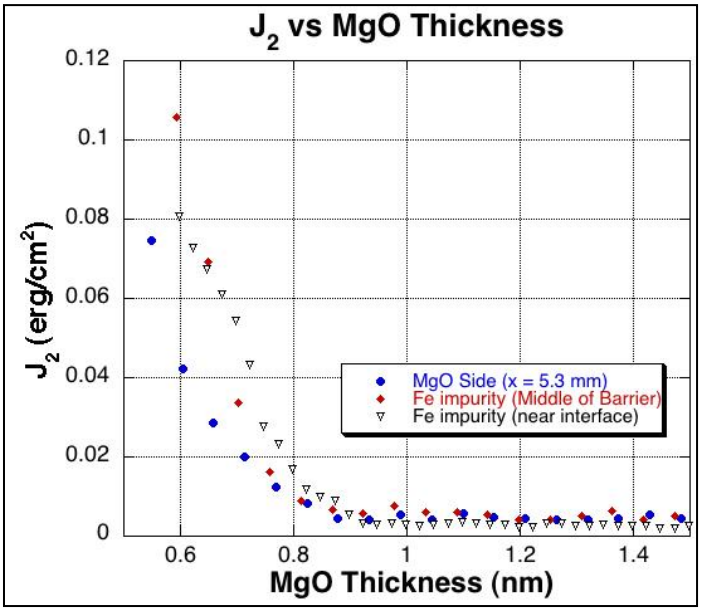

Figure 4- This is a graph of biquadratic coupling strength, J_2, versus the thickness of the MgO wedge.

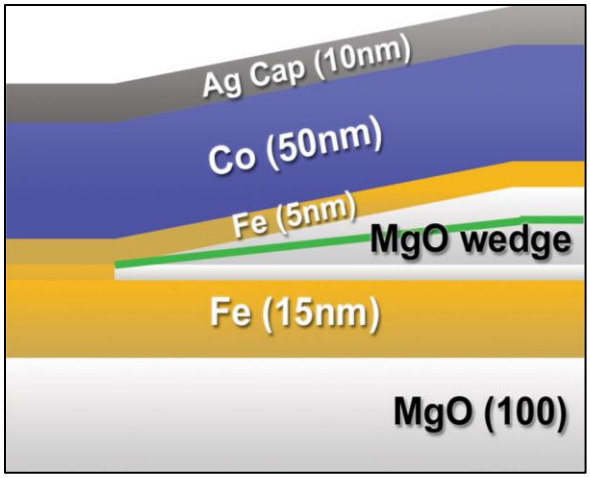

Figure 5- This is a diagram of a cross-section of a sample. This particular sample has the iron impurities (denoted by the green) in the middle of the wedge spacer.

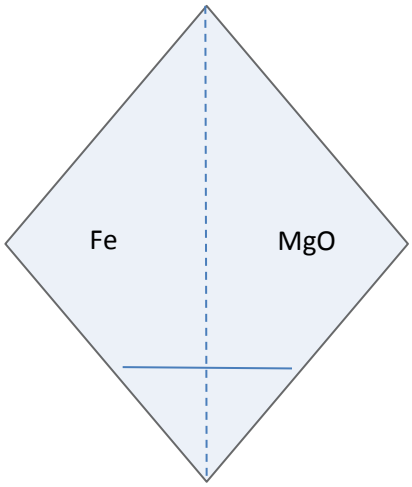

Figure 6- This shows the half/half wedge. On the left-hand side the iron impurities are in the middle of the wedge, and on the right-hand side there are no impurities. The wedge is directed from top to bottom, so the two halves are symmetric excepting the impurities.

[1] M. D. Stiles, J. Magn. Magn. Mater. 200, 322 (1999).
[2] M.Ye. Zhuravlev, J. Velev, A.V. Vedyayev and E.Y. Tsymbal. J. of Magn. Magn. Mater. Volume 300, Issue 1, May 2006, Pages e277-e280.
[3] J. Faure-Vincent, C. Tiusan, C. Bellouard, E. Popova, M. Hehn, F. Montaigne, and A. Schuhl, Phys. Rev. Lett. **89**, 107206 2002.
[4] P. G. Mather, J. C. Read, R. A. Buhrman. Phys. Rev. B **73**, 205412 (2006).
[5] M. Y. Zhuravlev, E. Y. Tsymbal, and A. V. Vedyayev, Phys. Rev. Lett. 94, 026806 (2005)
[6] Y. F. Chiang, Jared J. I. Wong, X. Tan, Yan Li, K. Pi, W. H. Wang, H. W. K. Tom, and R. K. Kawakami. Physical Review B 79, 184410 (2009).
[7] C. Tusche, H. L. Meyerheim, N. Jedrecy, G. Renaud, and J. Kirschner, Phys. Rev. B 74, 195422
(2006).
[8] Jared J. I. Wong, Luciana Ramirez, A. G. Swartz, A. Hoff, Wei Han, Yan Li, and R. K. Kawakami. Phys. Rev. B 81, 094406 (2010).